Quaternary faulting history along the Deep Springs fault, California

Jeffrey Lee*
Department of Geological Sciences, Central Washington University, Ellensburg, Washington 98926, USA and Institute for Crustal Studies, University of California, Santa Barbara, California 93106, USA

Charles M. Rubin
Department of Geological Sciences, Central Washington University, Ellensburg, Washington 98926, USA

Andrew Calvert
Department of Geological Sciences, University of California, Santa Barbara, California 93106, USA

ABSTRACT

New geologic mapping, structural studies, geochronology, and diffusion erosion modeling along the Deep Springs fault, California, shed light on its Quaternary faulting history. The Deep Springs fault, a 26-km-long, predominantly north-northeast-striking, west-northwest−dipping normal fault bounding the eastern side of Deep Springs Valley, cuts Jurassic batholithic rocks nonconformably overlain by middle Miocene to Pleistocene stream gravels, coarse-grained sand, tuffaceous sand, unwelded to partially welded tuff, and Bishop ash, as well as Quaternary coarse- to fine-grained alluvial fan deposits. The $^{40}Ar/^{39}Ar$ geochronology yields ages of 3.09 ± 0.08 Ma for the unwelded tuff and 753 ± 4 ka for the Bishop ash. Holocene debris flows, a landslide, and recent alluvium bury the youngest fault scarp. The Deep Springs fault is characterized by multiple fault planes and fault scarps that become progressively younger toward the basin. The dip of the fault plane varies from 20° to 87° and fault-plane and striation measurements indicate an average orientation of N23E, 47NW, and N77E, 49SW, respectively. The offset of Bishop ash and underlying tuff across the Deep Springs fault indicates horizontal extension and vertical slip rates of ~0.7 and ~0.9 mm/yr, respectively, since the eruption of the Bishop Tuff, and ~0.2 and ~0.2 mm/yr, respectively, since the eruption of the unwelded tuff. If the vertical slip rate since the eruption of the Bishop Tuff has remained constant through time, then slip along the Deep Springs fault began ca. 1.7 Ma. Younger fault scarps to the west of the bedrock fault cut Quaternary deposits; scarp offset ranges from 0.8 to 17.5 m and scarp slope angle ranges from 8° to 37°. Topographic profiling of the smallest, least eroded fault scarps, with an average surface offset of 2.7 m, indicates that these scarps developed as the result of a single earthquake and ruptured an ~20-km-long segment of the fault. Radiocarbon analyses on detrital charcoal, located in the footwall block of one of these scarps, yield an age of 1.960 ± 0.055 ka. Diffusion erosion modeling of these fault scarps yields an elapsed time of 1.7 ± 0.5 k.y. since these fault scarps formed. Making reasonable assumptions about the depth of this earthquake and shear modulus, we estimate a moment magnitude, $M_w \approx 7.0$, for this earthquake. The Deep Springs fault is one of several displacement-transfer normal faults that define a zone of distributed deformation between subparallel right-lateral strike-slip faults east of the Sierra Nevada that make up the northern part of the eastern California shear zone. The young age and recent earthquake activity along the Deep Springs fault are consistent with a model proposed for the kinematic evolution of this part of the eastern California shear zone.

Keywords: active faults, active tectonics, argon-argon, fault scarps, mapping, normal faults, structure, tectonics.

INTRODUCTION

Recent geologic and geodetic data indicate that a zone of right-lateral shear within eastern California and western Nevada is an important component of deformation within the Pacific−North America plate boundary zone, accounting for ~24% of the total relative plate motion (Dokka and Travis, 1990b; Humphreys and Weldon, 1994; Sauber et al., 1994; Savage et al., 1990). This zone, defined by Dokka and Travis (1990a) as the eastern California shear zone, extends from faults within the Mojave Desert northward to a zone of right-lateral strike-slip and normal faults east of the Sierra Nevada (Fig. 1A). Dokka and Travis (1990a) suggested that activity within the eastern California shear zone began between 20 and 6 Ma, and possibly as late as 10–6 Ma.

In spite of its tectonic importance, the space-time evolution of much of the eastern California shear zone remains poorly characterized. For example, geologic data suggest that right-lateral shear east of the Sierra Nevada was concentrated along the Death Valley fault system prior to 1 Ma; estimated late Miocene to Pleistocene slip rates were ≥3.5 mm/yr (Butler et al., 1988; Dokka and Travis, 1990a). Fault scarps along the Death Valley fault system cut Holocene deposits (Butler et al., 1988; Wills, 1989; Brogan et al., 1991), indicating that it is still active, but Holocene slip rates are unknown. Geologic studies show Holocene slip rates of ~2 mm/yr along the Owens Valley fault zone (Beanland and Clark, 1994) and a long-term slip rate of ~5 mm/yr since late Miocene time along the Fish Lake Valley fault zone. Estimated slip rates along the most active, central part of this fault zone are ~6−3 mm/yr from late Miocene to early Pleistocene time, ~11 mm/yr during middle Pleistocene time, and ~4 mm/yr (range of 1.9−9.3 mm/yr) since late Pleistocene time (Reheis and Sawyer, 1997).

A viscoelastic coupling model of spaced-based geodetic data across the Owens Valley

*E-mail: jeff@geology.cwu.edu.

GSA Bulletin; July 2001; v. 113; no. 7; p. 000–000; 10 figures; 3 tables.

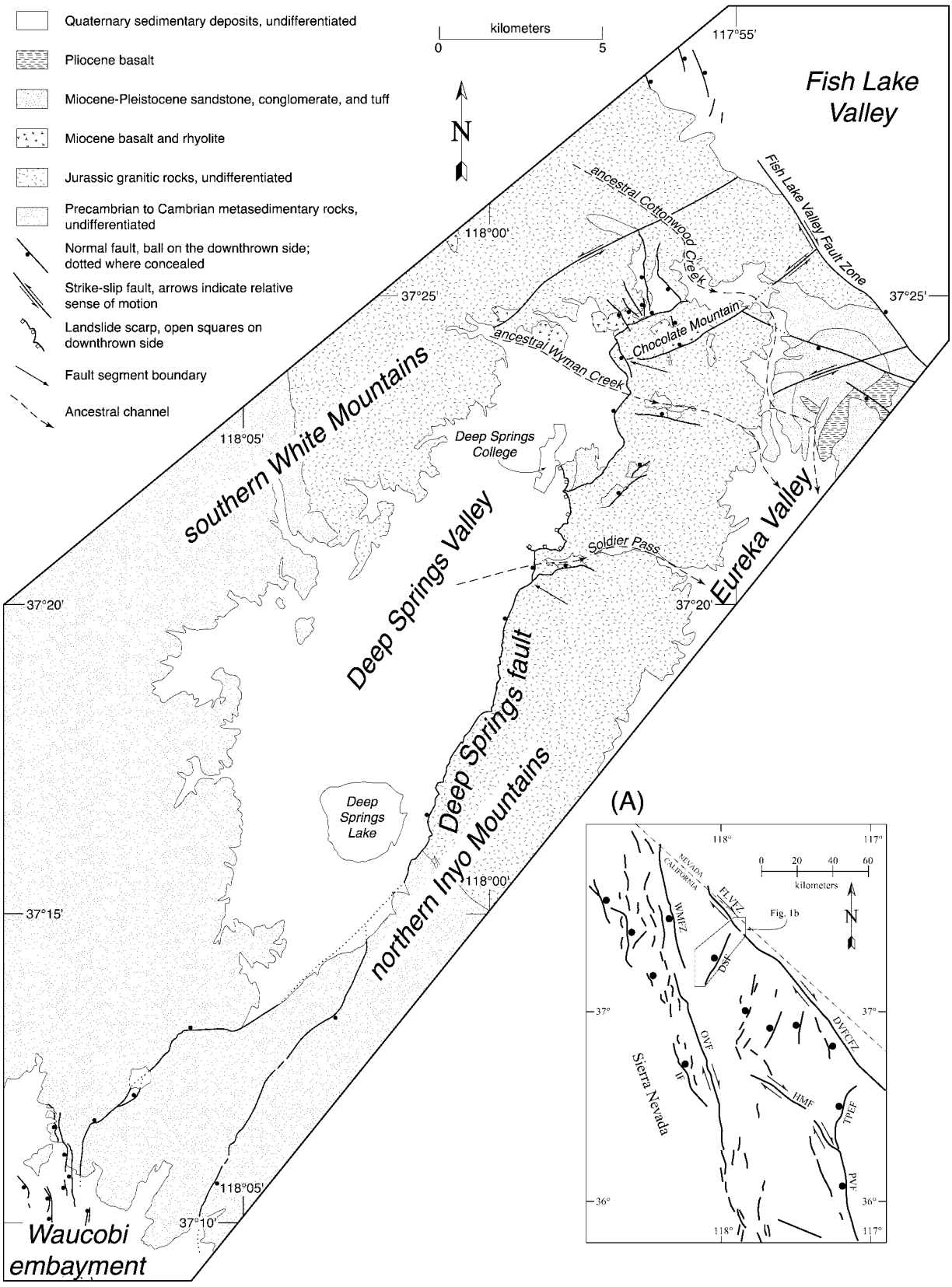
(B)
EXPLANATION
Quaternary sedimentary deposits, undifferentiated
Pliocene basalt
Miocene-Pleistocene sandstone, conglomerate, and tuff
Miocene basalt and rhyolite
Jurassic granitic rocks, undifferentiated
Precambrian to Cambrian metasedimentary rocks, undifferentiated
Normal fault, ball on the downthrown side; dotted where concealed
Strike-slip fault, arrows indicate relative sense of motion
Landslide scarp, open squares on downthrown side
Fault segment boundary
Ancestral channel
kilometers
0
5
N
117°55'
Fish Lake Valley
ancestral Cottonwood Creek
Fish Lake Valley Fault Zone
118°00'
37°25'
Chocolate Mountain
ancestral Wyman Creek
118°05'
southern White Mountains
Deep Springs College
Deep Springs Valley
Soldier Pass
Eureka Valley
37°20'
Deep Springs fault
Deep Springs Lake
northern Inyo Mountains
37°15'
118°00'
118°05'
37°10'
Waucobi embayment
(A)
118°
117°
0
20
40
60
kilometers
NEVADA
CALIFORNIA
FLVFZ
WMFZ
Fig. 1b
N
DSF
37°
DVFCFZ
OVF
IF
HMF
TPEF
PVF
Sierra Nevada
36°

fault zone and the Fish Lake Valley fault zone north of 37°N indicate present-day slip rates of 3.0 ± 1.9 mm/yr and 8.4 ± 2.0 mm/yr, respectively (Dixon, et al., 2000). Both of these present-day slip rates are the same, within error, to geologically determined Holocene to late Pleistocene slip rates for these faults. In contrast, south of 37°N, an elastic half-space model of geodetic data yields a summed slip rate of 5 ± 1 mm/yr across the Death Valley and Hunter Mountain fault systems (Bennett et al., 1997). These relations imply that deformation at the north end of the Owens Valley fault zone becomes more diffuse and/or steps right onto the Fish Lake Valley fault zone (Dixon et al., 1995; Savage and Lisowski, 1984; Savage et al., 1990; Wang et al., 1994).

There is an apparent paradox: geologic data require that the principal locus of shear averaged over the past few million years is the Death Valley−Furnace Creek fault zone. Yet conventional and space-based geodetic data suggest that the Fish Lake Valley fault zone is, at present, the principal locus of shear. A recently proposed model for the eastern California shear zone between lat 36° and 38° (Fig. 1A) explains this paradox by suggesting that the kinematic framework of this zone is changing very rapidly (Dixon et al., 1995). In this kinematic model, the locus of right-lateral shear has shifted or is in the process of shifting from the southern Death Valley fault zone to the Owens Valley fault zone. Furthermore, the model suggests that northeast-striking, northwest-dipping normal faults, such as the Deep Springs fault, Eureka Valley faults, and Towne Pass−Emigrant fault system, transfer slip from the Owens Valley and Hunter Mountain−Panamint Valley fault zones to the northern Death Valley−Furnace Creek and Fish Lake Valley fault zones.

This paper focuses on the Quaternary faulting and earthquake geology along one of these displacement-transfer normal faults, the Deep Springs fault, to assess its kinematic role in the evolution of the eastern California shear zone. We report on new detailed geologic mapping, structural, diffusion erosion modeling, and geochronologic investigations of the Deep Springs fault to characterize the geometry, kinematics, fault slip rate, and timing of fault motions.

GEOLOGY OF DEEP SPRINGS VALLEY

Regional Setting and Previous Work

The Deep Springs valley is an ~24-km-long, closed basin located between the southern White Mountains and the northern Inyo Mountains (Fig. 1B). The mountains surrounding the valley are underlain by deformed Precambrian to Cambrian sedimentary and metasedimentary rocks that were intruded by Jurassic granitic plutons. Tertiary basalt, tuff, and sedimentary rocks are exposed at the northern end of the valley. Quaternary alluvium and colluvium deposits cover the main part of the valley.

Miller (1928) was the first to recognize the youthful nature of the Deep Springs fault, noting the presence of well-developed triangular facets, offset Quaternary lavas, fault scarps developed across alluvial fans, and river gravels and boulders exposed in the footwall of the Deep Springs fault. Miller interpreted the river gravels and boulders as the ancestral Wyman Creek draining eastward into Eureka Valley (Fig. 1B). Lustig (1965) observed carbonate-cemented conglomerate in Soldier Pass, which he also interpreted to represent a former creek that drained eastward into Eureka Valley. Lustig (1965) likewise concluded that gravels south of Chocolate Mountain, first identified by Miller (1928), contained lithologies exposed in the southern White Mountains, and therefore the gravel source was to the west. Nelson (1966a, 1966b) and McKee and Nelson (1967) mapped the geology of the Deep Springs Valley region, but focused on the bedrock geology; their maps show that the Deep Springs fault cuts Quaternary deposits.

Wilson (1975) completed geophysical studies (seismic refraction, gravity, and magnetic studies) across the northern edge of Deep Springs Lake. He concluded that plutonic rocks and Precambrian to Cambrian sedimentary rocks (i.e., basement) in the hanging wall are currently as much as 795 m below the present valley floor and that the fault dips ~40°–45° toward 295°. The footwall at Deep Springs Lake, underlain solely by granitic basement, rises about 870 m above the valley floor, yielding a minimum vertical offset of 1665 m across the fault. This estimate is compatible with a measurement of 1250–1450 m of stratigraphic throw of Cambrian strata across the Deep Springs fault located in the northern Inyo Mountains southwest of Deep Springs Lake (C. Nelson, 1996, personal commun.).

Bryant (1989) completed detailed reconnaissance of aerial photographs and some field checking along the Deep Springs fault. He noted additional geomorphic features, such as wineglass-shaped drainages, fault scarps in young alluvial fans, and vertically offset drainages, that point to a young age for the Deep Springs fault. Preliminary scarp degradation modeling of two young fault scarps, using the SLOPEAGE program of D.B. Nash, yielded a 1.5−6 ka age for the most recent displacement along the fault. Bryant (1989) estimated a minimum vertical slip rate of 0.24 mm/yr along the northern part of the Deep Springs fault on the basis of stream-rounded pumice fragments tentatively correlated to the Bishop Tuff found in the footwall south of Chocolate Mountain.

Reheis and Sawyer (1997) identified three wind gaps containing well-rounded stream gravels in Deep Springs Valley. They confirmed the presence of the ancestral Wyman Creek and Soldier Pass drainage systems (i.e., Lustig, 1965; Miller, 1928) and identified a new ancestral drainage, Cottonwood Creek (Fig. 1). On the basis of lithologies and topographic position, Reheis and Sawyer corroborated Miller's (1928) and Lustig's (1965) interpretation that these deposits were formed by streams flowing eastward from the southern White Mountains into Eureka Valley. Because the stream deposits in the ancestral Wyman and Cottonwood Creek wind gaps are overlain by reworked Bishop ash, Reheis and Sawyer (1997) concluded that movement along the Deep Springs fault was not sufficient to defeat the flow of these drainages until after the eruption of the Bishop Tuff (753 ± 4 ka, see following). Assuming that the offset of stream gravels south of Chocolate Mountain is as much as twice their present-day

Figure 1. (A) Major Quaternary faults in the northern part of the eastern California shear zone. Fault abbreviations: DSF—Deep Springs fault, DVFCFZ—Death Valley−Furnace Creek fault zone; FLVFZ—Fish Lake Valley fault zone; HMF—Hunter Mountain fault; IF—Independence fault; OVF—Owens Valley fault; PVF—Panamint Valley fault; TPEF—Towne Pass−Emigrant fault system; WMFZ—White Mountains fault zone. (B) Simplified geologic index map of the Deep Springs Valley area. Sources of mapping are Nelson (1966a, 1966b), McKee and Nelson (1967), Reheis (1992), and this work.

height above the valley floor, Reheis and Sawyer (1997) calculated vertical slip rates of 0.3–0.5 mm/yr along the northern end of the Deep Springs fault since eruption of the Bishop Tuff.

Methods of Study

Geologic mapping on 1:24 000 scale aerial photographs and topographic base, and locally on a 1:1000 scale topographic base created using a Wild total station, and standard stratigraphic and structural field investigations reported here were augmented with $^{40}Ar/^{39}Ar$ and radiocarbon geochronology and diffusion erosion modeling of the youngest fault scarps. Geochronology was used to date volcanic rocks and alluvial fan deposits and, along with diffusion erosion modeling, was used to date the timing of faulting and earthquake activity. Results of argon isotopic analyses are listed in Table 1 and results of radiocarbon analyses are listed in Table 2, and age spectra are shown later in Figure 4. Diffusion erosion modeling was completed on topographic profiles, measured using a Wild total station, of representative fault scarps. Results of diffusion erosion modeling are listed in Table 3. Measured fault scarps are shown later in Figure 7, and calculated age results are shown later in Figure 9.

Rock Units and Ages

The basement exposed within the uplifted footwall of the Deep Springs fault consists of Jurassic monzonite plutonic rocks and deformed Precambrian to Cambrian sedimentary and metasedimentary rocks (Figs. 1B and 2A) (McKee and Nelson, 1967; Nelson, 1966a, 1966b). Nonconformably overlying the basement at the northern end of the valley are late Miocene olivine to pyroxene + olivine phyric basalt flows, which we informally refer to as Tertiary basalt, Tb, with hyaloclastite, basalt cinder, biotite + sanidine + quartz-bearing pumiceous rhyolite tuff, and granitic sand locally exposed at the base (Figs. 1B and 2A). K/Ar geochronology on whole-rock basalt yields an age of 10.8 Ma (Dalrymple, 1963) for this unit.

Exposed elsewhere at the northern end of the valley is a sedimentary section of well-bedded, granite-derived angular to subrounded, coarse sand supporting angular to subrounded quartzite and sandstone, metasedimentary, metavolcanic, granitic, vein quartz, and rhyolite tuff pebble- to boulder-sized clasts, and distinctive, scarce, small euhedral, transparent, colorless quartz crystals, which nonconformably overlie basement (Figs. 1B and 2A). Locally, the clast composition is solely limestone and dolomite. Approximately 140 m above the base of this unit is a ~5–10-m-thick distinct, white marker horizon composed of unwelded to partially welded, plagioclase- and quartz-bearing pumiceous tuff. Above the tuff is a tuffaceous sandstone composed of coarse sand and fine pebble-sized vein quartz clasts. Exposed near the top of this section, east of Deep Springs College, are massive tephra deposits >1 m thick. Although the base and top of the tephra are covered by younger alluvium and colluvium, we infer that the tephra is conformable with the rest of the unit because it appears that the same tuffaceous and granite-derived sand-

TABLE 1. ISOTOPIC ANALYSES OF DATED $^{40}Ar/^{39}Ar$ SAMPLES

Temperature (°C)	$^{40}Ar^{\dagger}$ (mol)	$^{40}Ar/^{39}Ar$	$^{37}Ar/^{39}Ar$	$^{36}Ar/^{39}Ar$	K/Ca	$^{39}Ar_k{}^{\S}$	$^{40}Ar^{\#}$	Age ± 1σ**
Sample: 95−5 plagioclase (J = 0.0007551)								
Total fusion age (TFA) = 3.91 ± 0.09 Ma								
Weighted mean plateau age (WMPA) = 3.09 ± 0.08 Ma								
Steps used: 975−1250, or 50% $\Sigma^{39}Ar$								
Inverse isochron age = 3.00 ± 0.25 Ma (MSWD = 9.6; $^{40}Ar/^{36}Ar$ = 335 ± 99)								
725	1.4e-14	95.7232	1.8237	0.0721	0.280	0.001	0.779	99.0 ± 6.5
800	1.7e-14	12.6108	1.6809	0.0326	0.304	0.014	0.248	4.26 ± 0.68
900	1.0e-14	3.7716	1.5783	0.0025	0.323	0.040	0.842	4.33 ± 0.29
975	2.2e-14	4.1040	1.5358	0.0067	0.332	0.091	0.549	3.07 ± 0.17
1050	3.9e-14	4.0961	1.4994	0.0056	0.340	0.181	0.626	3.49 ± 0.11
1150	3.7e-14	2.5765	1.4919	0.0014	0.342	0.317	0.892	3.13 ± 0.06
1250	6.5e-14	2.7424	1.3956	0.0022	0.366	0.542	0.804	3.01 ± 0.04
1350	4.5e-14	6.6319	1.3977	0.0096	0.365	0.606	0.589	5.32 ± 0.16
1650	1.9e-13	4.6730	1.4257	0.0056	0.358	1.000	0.673	4.28 ± 0.03
Sample: 95−28 sanidine (J = 0.0001945)								
Total fusion age (TFA) = 757 ± 5 ka								
Weighted mean plateau age (WMPA) = 753 ± 4 ka								
Steps used: 900−1300, or 94% $\Sigma^{39}Ar$								
Inverse isochron age = 753 ± 5 ka (MSWD = 0.39; $^{40}Ar/^{36}Ar$ = 287.1 ± 11.6)								
700	8.5e-15	2.6026	0.0452	0.0116	11	0.016	0.431	913 ± 67
800	8.5e-15	2.2537	0.0338	0.0041	14	0.043	0.649	791 ± 37
900	1.3e-14	2.1138	0.0251	0.0023	19	0.094	0.760	742 ± 19
1000	2.1e-14	2.1329	0.0165	0.0011	30	0.186	0.866	748 ± 11
1050	1.9e-14	2.1287	0.0115	0.0007	43	0.273	0.908	747 ± 11
1080	1.2e-14	2.1585	0.0087	0.0005	56	0.329	0.934	757 ± 18
1100	1.1e-14	2.1302	0.0092	0.0005	53	0.381	0.931	747 ± 18
1130	1.1e-14	2.1535	0.0071	0.0003	69	0.433	0.956	756 ± 19
1170	1.8e-14	2.1420	0.0066	0.0003	74	0.524	0.960	752 ± 11
1220	5.2e-14	2.1482	0.0069	0.0002	71	0.782	0.978	754 ± 5
1300	4.3e-14	2.1476	0.0067	0.0001	73	1.000	0.985	754 ± 5
Sample: 95−37 sanidine (J = 0.0001948)								
Total fusion age (TFA) = 756 ± 34 ka								
1300	5.4e-15	2.1520	0.0106	0.0014	46	1.000	0.836	756 ± 34
Sample: 95−66 sanidine (J = 0.0001951)								
Weighted mean age = 15.1 ± 0.1 Ma								
1300	9.7e-14	43.1182	0.0067	0.0037	73	1.000	0.975	15.1 ± 0.1
1300	5.3e-14	42.9056	−0.0066	0.0011	<0.001	1.000	0.992	15.0 ± 0.1
1300	5.8e-14	43.0072	0.0075	0.0011	65	1.000	0.993	15.1 ± 0.1
1300	9.8e-14	43.2195	0.0040	0.0008	123	1.000	0.995	15.1 ± 0.1
1300	8.4e-14	42.8450	−0.0075	0.0015	<0.001	1.000	0.990	15.0 ± 0.1

Note: MSWD—mean square of weighted deviates; expresses the goodness of fit of the isochron.

*Mineral separates were obtained using magnetic separatory methods, paper shaking, heavy liquids, and hand-picking to >99% purity. $^{40}Ar/^{39}Ar$ samples 95−28, 95−37, and 95−66 were wrapped in copper foil, placed in evacuated quartz vials with flux monitor Fish Canyon Tuff sanidine (assumed age = 27.8 Ma) and irradiated at the TRIGA reactor, Oregon State University. These samples were analyzed at the University of California, Santa Barbara, by step-heating or total fusion in a Ta crucible within a double-vacuum Staudacher-type resistance furnace, gettered by two SAES ST-172 porous getters and analyzed on a MAP 216 mass spectrometer fitted with a Baur-Signer source and a Johnston MM1 multiplier with a sensitivity of 2.0×10^{-14} moles/volt. Temperatures were monitored with a tungsten-rhenium thermocouple to ±5 °C. Typical extraction line blanks vary from 2.0×10^{-16} moles ^{40}Ar at <1000 °C to 6.0×10^{-16} moles ^{40}Ar at 1300 °C. $^{40}Ar/^{39}Ar$ sample 95−5 was placed in a machined Al disc and irradiated, along with flux monitor Fish Canyon Tuff sanidine, at the Nuclear Science Center reactor, Texas A&M University. Sample was analyzed at New Mexico Bureau of Mines and Mineral Resources by step-heating in a Mo double-vacuum resistance furnace, gettered by 3 SAES GP-50 getters and a tungsten filament operated at ~2000 °C, and analyzed on a MAP 215−50 mass spectrometer on line with automated all-metal extraction system and a Johnston electron multiplier with a sensitivity of 2.21×10^{-16} moles/pA. Temperature was monitored with a tungsten-rhenium thermocouple and the furnace system blank was 1.3×10^{-14} moles ^{40}Ar at <1300 °C. Errors reported are 1σ. See Hacker (1993) for method of calculating isotopic abundances, corrections and uncertainties. Weighted mean plateau ages (WMPA) are reported where ≥50% of the ^{39}Ar released in contiguous steps is within 1σ error.

$^{\dagger}{}^{40}Ar$ (mol): ^{40}Ar moles corrected for blank and reactor-produced ^{40}Ar.

$^{\S}\Sigma^{39}Ar$: cumulative ^{39}Ar released.

$^{\#}{}^{40}Ar^*$: radiogenic fraction of ^{40}Ar.

**Age in ka for samples 95−28 and 95−37, and Ma for samples 95−5 and 95−66.

TABLE 2. RADIOCARBON ANALYSES OF CHARCOAL AND TREE SAMPLES

Sample number	Stratigraphic unit	^{14}C age (yr B.P. ± 1σ)	Calendar age range*
95–78b	Qdf	445 ± 55	A.D. 1405–1630
95–54c	Qf1	1,960 ± 55	50 B.C.–A.D. 206

Note: Samples are listed in stratigraphic order. Reported ^{14}C ages use Libby's half-life (5568 yr).
*Dendrochronogically calibrated calendar ages were calculated using Stuiver and Reimer (1993), Method B, 20 yr. calibration curve, and 2σ uncertainty. Calendar year ages are radiocarbon ages corrected for the reservoir effect (Stuiver and Pollach, 1977) and for these samples the calibration relies on radiocarbon dates from tree rings of known ages.

stones continue above the tephra. Exposures of this ~280-m-thick unit, informally referred to as Tertiary–Quaternary sand,TQs, are both in the hanging wall and footwall of the Deep Springs fault east of Deep Springs College (Figs. 2A and 3). In addition, in the footwall just south of Chocolate Mountain to Soldier Pass region, this unit includes deposits of rounded pebble- to boulder-sized granite, metasedimentary, metavolcanic, and volcanic clasts that also nonconformably overlie the basement. Because most of these deposits are in wind gaps, they have been interpreted as stream gravels exposed along the ancestral Wyman and Cottonwood Creeks and in Soldier Pass (Lustig, 1965; Miller, 1928; Reheis and Sawyer, 1997) (Figs. 1B and 2A). Scarce exposures of cross-bedding and pebble imbrication indicate eastward transport, supporting the interpretations of Miller (1928), Lustig (1965), and Reheis and Sawyer (1997) that these ancestral drainages flowed eastward into Eureka Valley. Total fusion of single grains of sanidine from a subrounded, biotite, pumice, and lithic-bearing rhyolite tuff boulder (sample 95–66) (Fig. 2A) within the basal conglomerate yields a weighted mean ^{40}Ar/^{39}Ar age of 15.1 ± 0.1 Ma (Table 1). A conventional ^{40}Ar/^{39}Ar step-heating experiment on a plagioclase separate from the tuff marker horizon (sample 95–5) (Fig. 2A) yields a weighted mean ^{40}Ar/^{39}Ar plateau age (WMPA) of 3.09 ± 0.08 Ma (Fig. 4; Table 1). A conventional ^{40}Ar/^{39}Ar step-heating experiment on a sanidine separate from the tephra exposed near the top of the unit and total fusion of a single sanidine grain from reworked tephra deposited upon gravel deposits along the Wyman ancestral creek (samples 95–28 and 95–37, respectively) (Fig. 2A) yields a WMPA of 753 ± 4 ka and an ^{40}Ar/^{39}Ar age of 756 ± 34 ka, respectively (Fig. 4; Table 1), indicating that these tephra deposits are the Bishop ash (cf. Izett and Obradovitch, 1994). These ages bracket the deposition of theTQs unit between middle Miocene and middle Pleistocene time.

Four distinct Pliocene (?) to Holocene alluvial fan deposits are exposed along the eastern side of Deep Springs Valley (Fig. 2A). Exposed at the southern end of the valley are unconsolidated fan deposits composed primarily of Precambrian quartzite boulders, informally termed boulder fanglomerate, Qbf, the source of which is due east in the footwall of the Deep Springs fault (Fig. 2A). This alluvial fan is largely deposited across and buries the southernmost exposures of the Deep Springs fault.

Remnants of a fan comprising weathered, subrounded to angular, poorly sorted, matrix-supported granitic clasts, referred to as Qf2, are exposed along the length of the Deep Springs fault. Clasts range in size from small cobbles to scarce 1 m boulders, and some exhibit incipient to moderate desert varnish on most surfaces. Weathered, angular, poorly sorted granitic silt to large pebbles compose the matrix. This alluvial fan is more dissected than Qf1 (see following).

The dominant alluvial fan deposits along the range front, referred to as Qf1, are generally coarse, granitic sand with lesser angular to subrounded granite-derived pebbles and boulders. A 1-cm-long piece of charcoal, found ~1 m below the surface of Qf1 west of Soldier Pass (sample 95–54c) (Fig. 2A), yields a radiocarbon age of 1.960 ± 0.055 ka (calendar age range of 50 B.C.–A.D. 205), indicating that this fan is early Holocene in age (Table 2). The youngest fault scarp developed along the Deep Springs fault cuts Qf1, indicating that this rupture event is younger than ca. 1.9 ka. Qf1 deposits interfinger with deposits of playa silt and clay, here called Qvf, and with fan gravel of mixed lithologies and sand derived from the southern flank of the White Mountains, here called Qfw.

Exposed along the range front to the southeast of Deep Springs College is a large, ~3 km^2, landslide composed solely of granitic debris (Fig. 2A). The landslide exhibits a well-developed head scarp, transverse cracks, and hummocky topography. Here, the height of the Deep Springs fault escarpment above the valley floor is ~275 m, considerably less than to the south, where it is ~870 m. The relatively low height of the footwall is consistent with the landslide originating at the top of the escarpment. The landslide has been deposited across the Deep Springs fault, the most recent fault scarps, and Qf1, indicating that it is younger than ca. 1.9 ka.

Narrow (to 30 m across) debris flows with well-defined levees, informally referred to as Qdf, are composed of angular to subangular granitic boulders typically 0.5 m across, but as much as 5 m across. Boulders are not varnished and are commonly light colored compared to their source, indicating relatively recent deposition. These debris flows are developed at the base of short, steep canyons in the footwall, and have been deposited across Qf1 and the youngest fault scarps developed along the Deep Springs fault. A piñon log (sample 95–78b) (Fig. 2A) deposited within Qdf yields a radiocarbon age of 0.445 ± 0.055 ka (age range of A.D. 1405–1630), indicating that these deposits are younger than ~480 yr (Table 2).

DEEP SPRINGS FAULT

Fault Geometry and Geomorphology

The Deep Springs fault is a 26-km-long, predominantly north-northeast–striking, west-northwest–dipping normal fault exposed along the eastern side of Deep Springs Valley (Figs. 1B and 2A). Basement rocks are exposed primarily within the footwall of the fault and Quaternary alluvial fan deposits are exposed primarily in the hanging wall. The height of the footwall escarpment above the valley floor ranges from a maximum of ~870 m to the east of Deep Springs Lake to a minimum of ~145 m in the Soldier Pass region (Figs. 1B and 2A). A relatively young age for the Deep Springs fault is indicated by (1) well-developed geomorphic features such as triangular facets and wineglass-shaped drainages; (2) fault scarps developed across young alluvial fans; (3) vertically offset drainages (Bryant, 1989; Miller, 1928); and (4) the steep escarpment, to 38° east and northeast of Deep Springs Lake.

The Deep Springs fault, which we define as the fault developed at the range front–piedmont interface that typically juxtaposes Tertiary and Quaternary sediments in the hanging wall on basement in the footwall, or Quaternary sediments in the hanging wall on Quaternary sediments in the footwall, is characterized by multiple fault planes and fault scarps. Fault planes, located east of fault scarps, are commonly either poorly exposed or strongly weathered; easternmost fault scarps are relatively heavily vegetated and westernmost fault scarps appear fresh and less

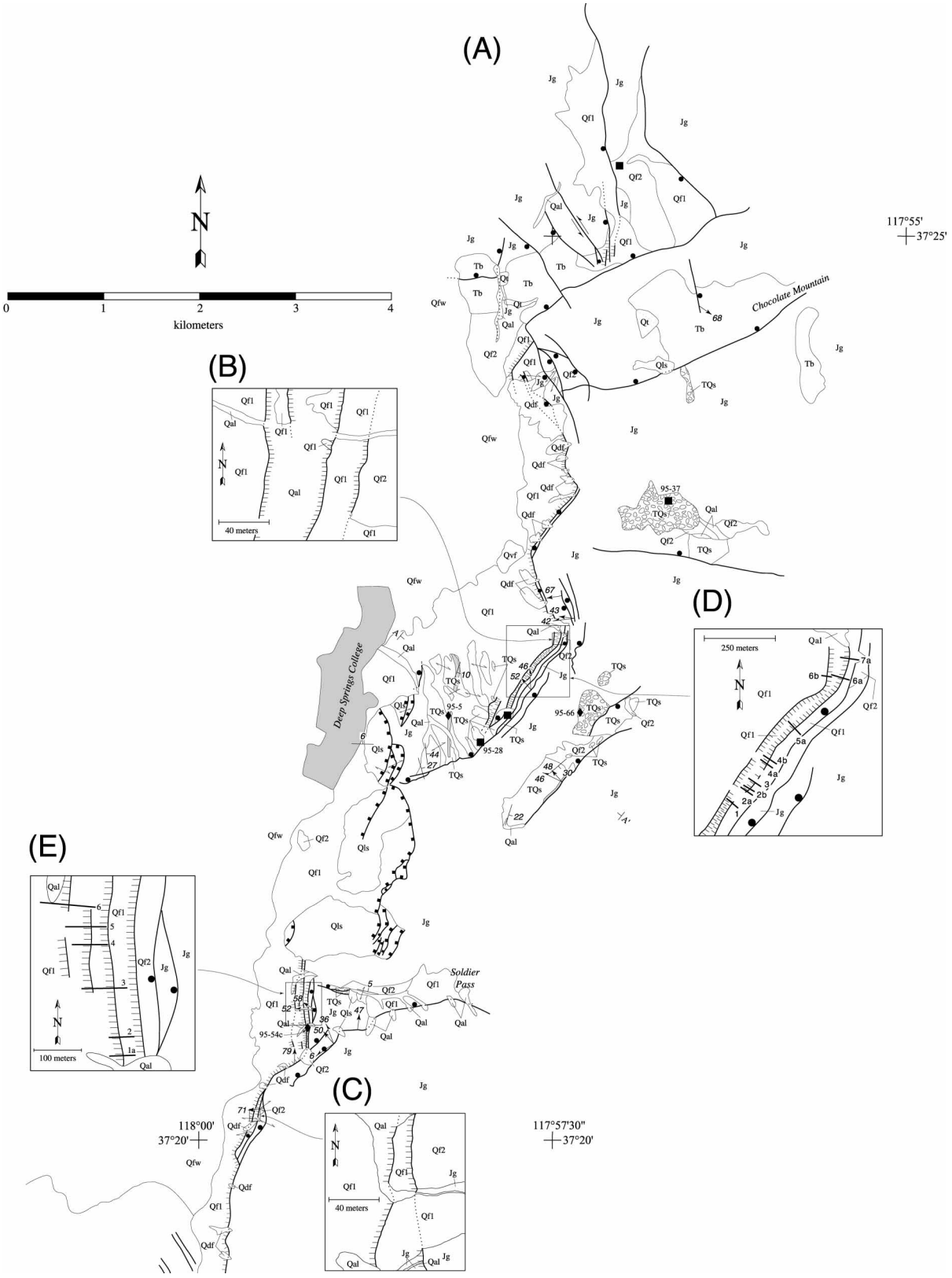

Figure 2. (A) Simplified geologic map of the Deep Springs fault. (B and C) Detailed geologic maps of selected localities along the Deep Springs fault showing that fault scarps young basinward. See text for discussion. (D and E) Detailed geologic maps showing locations of profiles (heavy lines) used for morphologic dating.

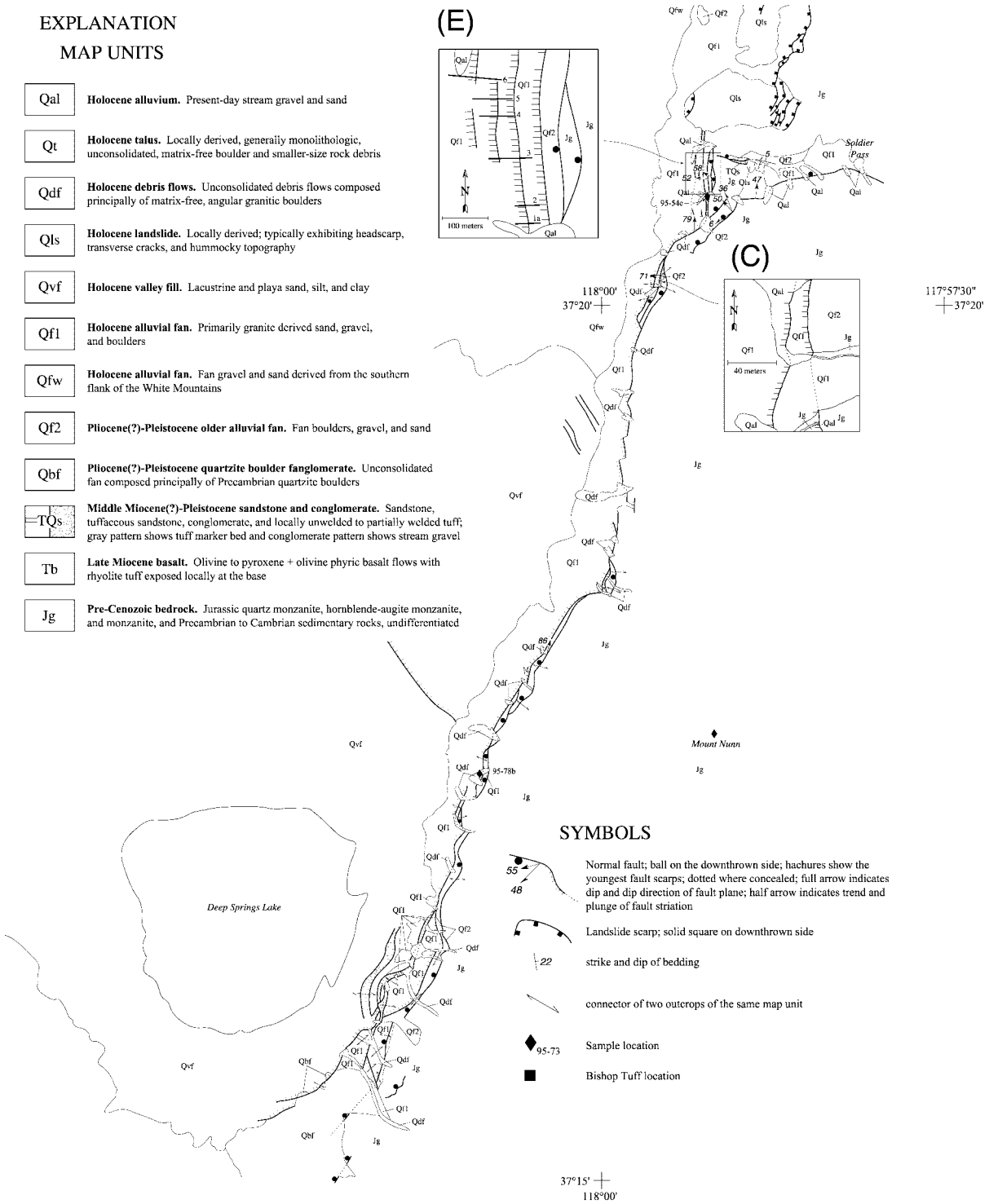

Figure 2. (*Continued***)**

vegetated. Furthermore, older fault scarps or faults to the east displace bedrock and Qf2, but not Qf1 and younger deposits, whereas younger fault scarps to the west displace Qf1, but often not older deposits such as Qf2 (Fig. 2, B and C). We interpret these relations to indicate that fault planes and fault scarps become progressively younger toward the sedimentary basin.

The oldest fault planes, exposed either within bedrock or at the bedrock−alluvial fan interface, locally expose fault surfaces and fault striae. The dip of the fault plane varies from 20° to 87° to the west; the average orientation is N23E, 47NW (Fig. 5A). Fault striations show a wider range in orientation and average N77E, 49SW (Fig. 5B). These older faults are characterized by a zone, as wide as

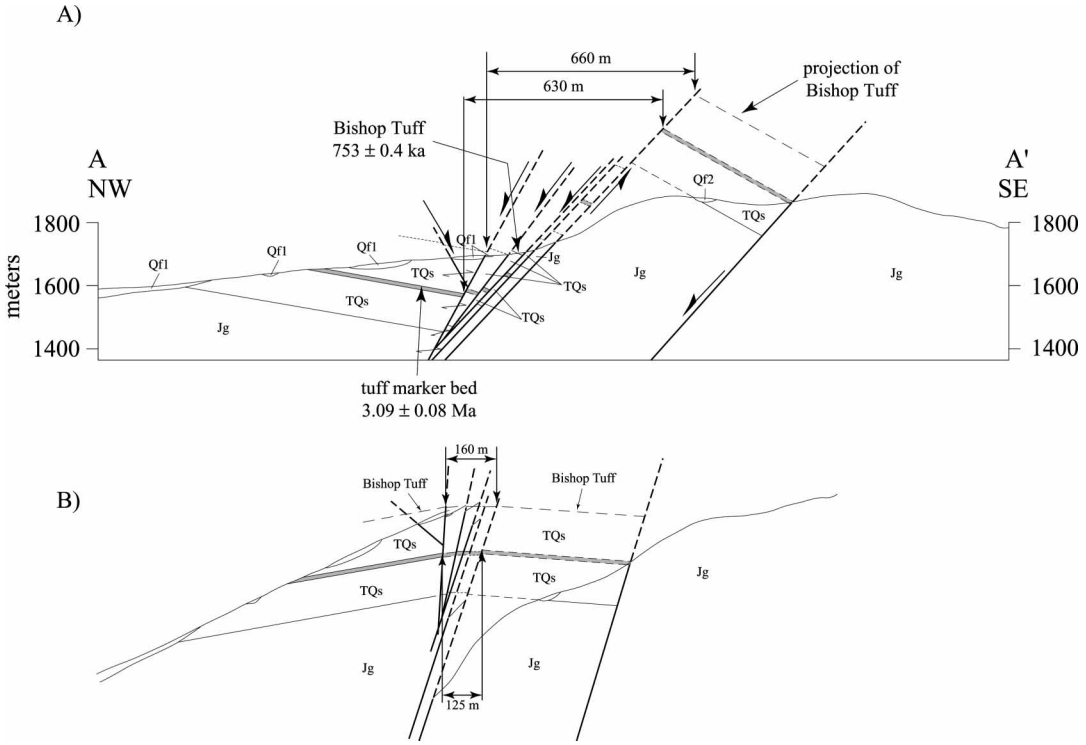

Figure 3. (A) Interpretative northwest-southeast cross-section A–A′ across the Deep Springs fault east of Deep Springs College. (B) Palinspastic restoration of cross section shown in A. See Figure 2 for location of cross section and abbreviations.

5 m, of extensively sheared, crushed, and fractured granite, and a zone of granite-derived cataclasite and fault gouge as wide as 80 cm. Scarce exposures indicate that the fault zone is cemented with calcium carbonate, but striations defined by linear ridges of caliche were observed in only a couple of exposures. West of Soldier Pass and east of Deep Springs College, silica-rich fluids deposited quartz along the fault planes. The quartz displays well-developed polished fault planes and fault striations defined by small mullions and grooves. Locally, the quartz is extensively brecciated into centimeter-sized angular pieces. There are also scarce exposures of millimeter- to centimeter-wide seams or zones of pseudotachylyte developed within footwall granitic rocks. Where exposed along the fault plane, the pseudotachylyte is polished and contains well-developed striations defined by grooves and small mullions.

A number of approximately east-west−striking, north-dipping cross-faults are exposed in the footwall in the Soldier Pass region, near the ancestral Wyman Creek wind gap, and Chocolate Mountain (Figs. 1 and 2). At the north end of the valley, the Deep Springs fault splays into a number of north-northwest− to SSE−striking normal faults. These faults and associated fault striations show a range of orientations (Fig. 5).

West- to northwest-dipping fault scarps are exposed along the length of the Deep Springs fault from north-northeast of Deep Springs College to southeast of Deep Springs Lake (Fig. 2A). The youngest set of fault scarps appears to die out northward into the Miocene basalt field and southward into Qbf. The fault scarps develop at the alluvial fan−bedrock interface, within Qf1 and Qf2 alluvial fan deposits, and within Qvf deposits. Thin (typically $<$1 m thick) colluvial deposits are along the base of the most recent fault scarps. These colluvial deposits are wedge shaped, indicating that they developed after the scarp-forming event. Surface offset or scarp offset (Fig. 6) ranges from 17.5 to 0.8 m and the scarp slope angle ranges from 8° to 37°. Two small grabens are to the east of Deep Springs College and along the eastern shoreline of Deep Springs Lake (Fig. 2, A and B). The latter follows the contours of the toes of alluvial fan deposits where these deposits interfinger with lacustrine sand, silt, and clay deposits (Fig. 2A). The surface offset across the fault scarps that bound these grabens is as much as 16.6 m; the development of these scarps may have been enhanced by spreading due to liquefaction of the lacustrine deposits (Bryant, 1989; Wills, 1996).

The Deep Springs fault can be subdivided into three geometric fault segments: south of Soldier Pass, Soldier Pass to west of Chocolate Mountain, and west of Chocolate Mountain northward (Figs. 1B and 2A). The fault segment south of Soldier Pass exposes a fairly linear north-northeast−striking fault trace and a narrow fault zone typically defined by one or two subparallel faults and fault scarps. The central segment between Soldier Pass and west of Chocolate Mountain shows a change from the south in the Soldier Pass area, where the fault zone is a relatively wide zone defined by as many as seven, approximately north-south−striking faults and fault scarps, to the north, where it is characterized by a relatively narrow zone defined by one to five subparallel faults and fault scarps with a strike of north-northwest or northeast. The boundary between this segment and the one to the south is a cross-fault boundary (e.g., Machette et al., 1991) defined by two approximately east-west−striking, north-dipping normal faults in the Soldier Pass region. The youngest fault scarps exposed in this segment ruptured across this boundary into the southern segment and ruptured ~0.5 km into the northern segment

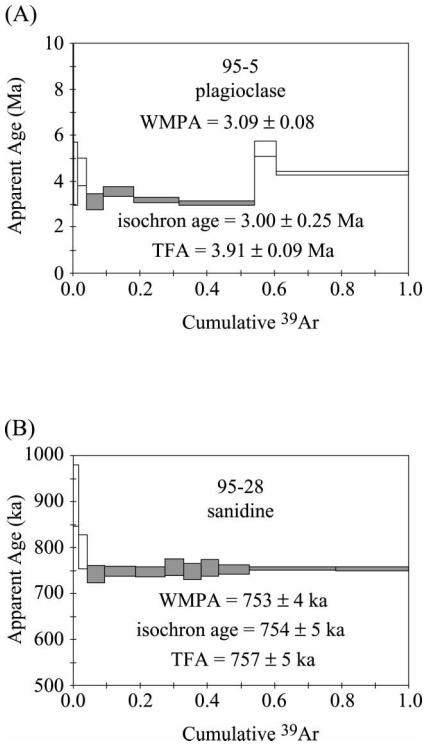

Figure 4. $^{40}Ar/^{39}Ar$ age spectra. (A) Sample 95–5, a plagioclase from a tuff marker horizon located within the middle of TQs (see Fig. 2). (B) Sample 95-28, a sanidine from a tephra deposit located near the top of TQs. Shaded steps are those used in determining the weighted mean plateau age (WMPA). TFA is total fusion age. See Figure 2A for locations of these samples.

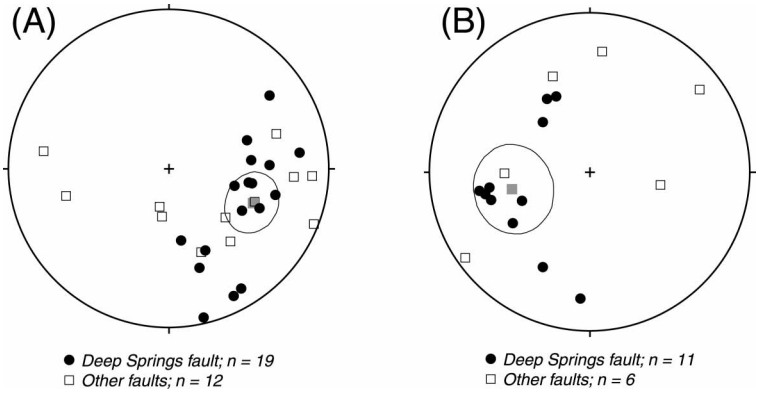

Figure 5. Structural data plotted on lower hemisphere, equal-area projections. Number of measurements indicated. (A) Poles to fault planes for the Deep Springs fault proper (solid circles) and other faults (open squares). (B) Trend and plunge of fault striations for the Deep Springs fault (solid circles) and other faults (open squares). Shaded square is the mean pole to Deep Springs fault planes (A) and mean trend and plunge for Deep Springs fault striations (B). Ellipses are 95% confidence cones for these mean orientations.

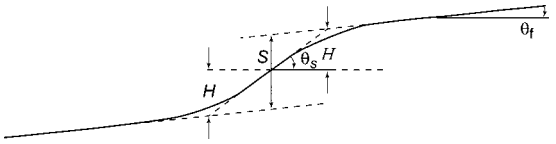

Figure 6. Geometry of a fault scarp after Hanks et al. (1984). Abbreviations: 2H, scarp height; S, surface offset or scarp offset; θ_f, far-field slope angle; θ_s, scarp slope angle.

(Fig. 2A). The geometry of the northern segment is characterized by changes in fault strike, from east-northeast to northwest, and a broad zone of normal faults. The boundary between this segment and the one to the south is also a cross-fault boundary defined by an east-northeast−striking, north-dipping normal fault just south of Chocolate Mountain.

Fault Kinematics, Magnitude of Fault Slip, and Slip Rates

The geometry of faulting and the dip of bedding define extension direction. The normal faults along the east side of Deep Springs Valley strike predominantly north-northeast and dip west-northwest, and what little bedding is exposed predominantly dips east-northeast to east-southeast, suggesting west-northwest−east-southeast extension (Fig. 2). Fault striations appear to indicate a small left-lateral component of slip along the Deep Springs fault (Fig. 5); however, because this

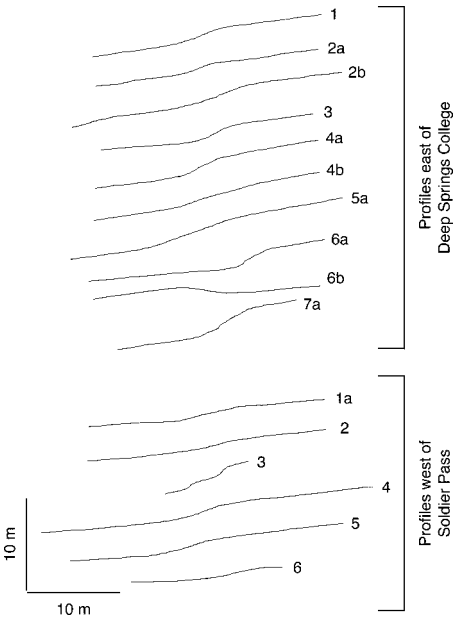

Figure 7. Measured profiles across fault scarps exposed east of Deep Springs College and west of Soldier Pass (see Fig. 2, D and E, for locations). Note that the scales for profiles 3 and 6 west of Soldier Pass are 50% and 25%, respectively, of that indicated.

data set is small, it most likely is not representative of the entire fault. Moreover, we do not observe any geomorphic evidence indicating a lateral component of slip, either along older faults or along younger fault scarps, suggesting a history of essentially dip slip along the Deep Springs fault.

The approximately west-northwest−east-southeast extension along the Deep Springs fault is transferred northeastward to the Fish Lake Valley fault zone along east-northeast−striking, left-lateral strike-slip faults (Reheis and Sawyer, 1997) (Fig. 1B). To the southwest, the fault bends into a series of north-south− to north-northwest−striking, west-dipping normal faults developed within the Waucobi embayment along the western flanks of the White and Inyo mountains (Fig. 1B).

We can estimate the magnitude and rate of fault slip along the southern and northern parts of the Deep Springs fault. East of Deep Springs College, a sequence of eastward tilted TQs with Bishop ash near its top nonconformably overlies Jurassic granite and has been offset across several faults of the Deep Springs fault zone, where fault dips range from 48° to 62° northwest (Figs. 2A and 3). We estimated the magnitude of extension by palinspastically

restoring the apparent downdip displacement along faults across a cross section east of Deep Springs College (Fig. 3, A and B). The magnitudes of horizontal extension since the eruption of the Bishop ash and tuff marker unit are ~500 m and ~505 m, respectively (Fig. 3, A and B). The uncertainty associated with these measurements is difficult to quantify; however, we believe it is no greater than ±5 m. Taking into account the uncertainties in age of the Bishop ash and the tuff marker unit yields a maximum and minimum horizontal extension rate of ~0.7 mm/yr and ~0.2 mm/yr, respectively, across the Deep Springs fault. Restoring bedding in the hanging wall and footwall to its original, approximately horizontal, orientation rotates the faults to a 73°–83° northwestward dip and yields vertical offsets across the faults of ~695 m (Bishop ash) and ~710 m (tuff marker bed). Vertical slip rates are ~0.9 mm/yr since eruption of the Bishop Tuff and ~0.2 mm/yr since the eruption of the tuff marker bed. These vertical slip rate estimates are maxima, because the fault and hanging wall and footwall blocks have rotated ~20° during slip. Our vertical slip rate estimates bracket the 0.3–0.5 mm/yr vertical slip rate estimate of Reheis and Sawyer (1997). Reworked Bishop ash overlies stream deposits in the ancestral Wyman and Cottonwood Creek wind gaps, indicating that there was insufficient movement along the Deep Springs fault that blocked drainage flow prior to the eruption of the Bishop Tuff (Reheis and Sawyer, 1997), or that not much movement occurred along the fault prior to the eruption of the tuff. Therefore the ~0.7 mm/yr and ~0.9 mm/yr horizontal and vertical slip rates, respectively, calculated here based on offset of the Bishop ash, are our preferred slip rate estimates for the northern part of the Deep Springs fault.

To the south, along the northern edge of Deep Springs Lake, the depth to basement in the hanging wall is ~795 m (Wilson, 1975) and the height of the escarpment is ~870 m, indicating a minimum vertical offset of 1665 m, at least 2.25 times that to the north. This implies that the vertical slip rate east of the lake is at least 2.25 times that to the north (i.e., ~2.0 mm/yr) or, if the vertical slip rate has remained constant along the length of the Deep Springs fault, then slip along this portion of the Deep Springs fault began ca. 1.7 Ma.

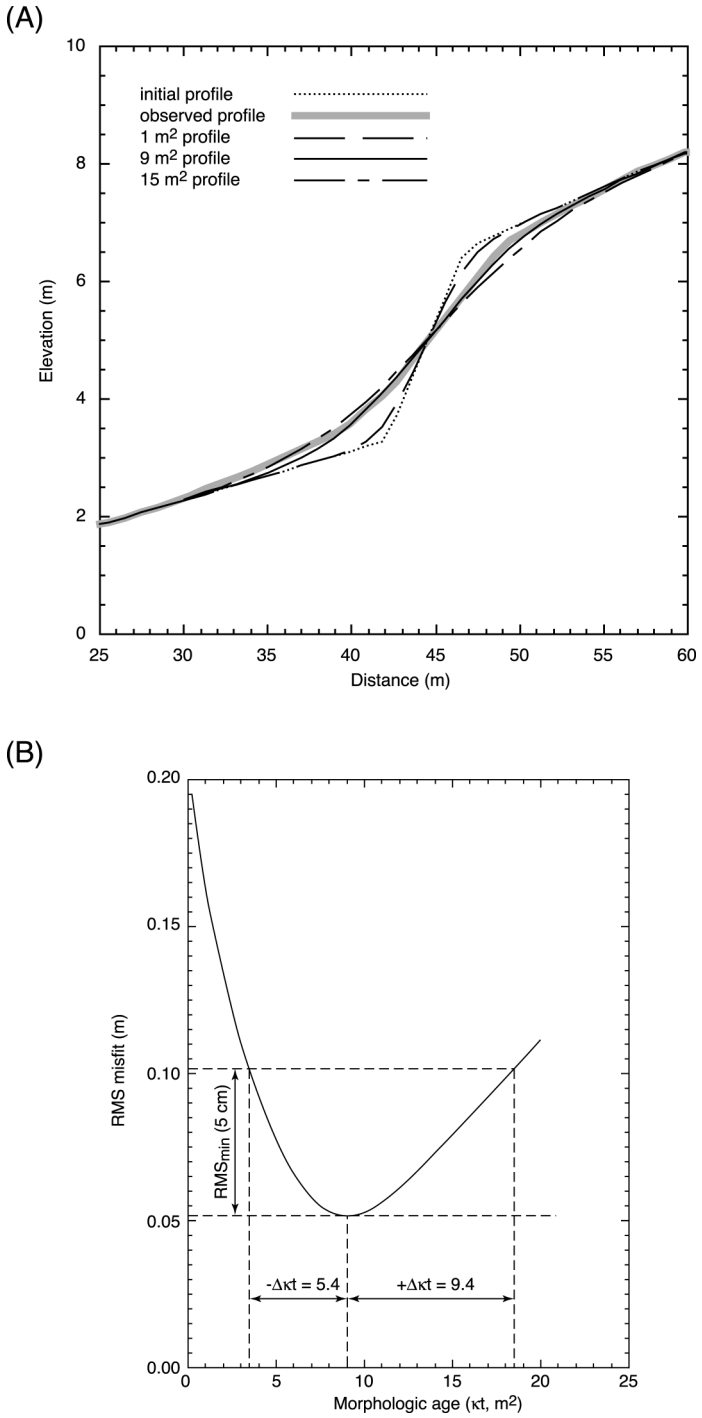

Figure 8. Example of diffusion erosion modeling results for profile 4 located west of Soldier Pass. (A) Elevation versus distance plot of observed profile (gray line), modeled profiles (best fitting, solid line; representative bracketing ones, dashed lines; numbers correspond to morphologic age), and initial shape (dotted line). (B) Corresponding plot of root mean square (RMS) misfit versus *κt*.

Morphologic Dating and Earthquake Magnitude

Recent fault scarps are well developed along the Deep Springs fault, particularly within unit Qf1 and at the interface between alluvial fan deposits and bedrock. Within alluvial fan deposits, present-day fault scarp angles range from 6° to 37° and measured scarp offsets range from 0.8 to 17.5 m. Those scarps with offsets >~4–5 m exhibit more than one knickpoint in profile, suggesting that they preserve evidence for more than one event.

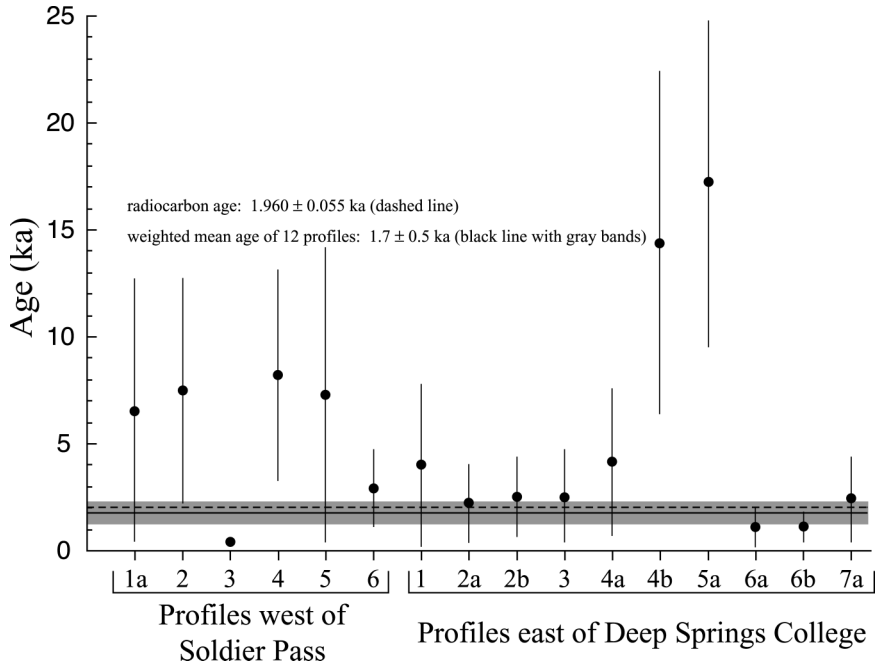

Figure 9. Morphologic dating results (calculated age ±1σ) for fault scarps along the Deep Springs fault west of Soldier Pass area and east of Deep Springs College (see Fig. 2, D and E, for locations). Weighted mean (mean of individual ages weighted inversely by their variance) of 12 topographic profiles yields an age of 1.7 ± 0.5 ka (error in age does not include uncertainty associated with κ determined for Lake Bonneville shoreline scarps nor its application to eastern California), within 1σ error of a radiocarbon age of 1.960 ± 0.055 ka on charcoal found in the footwall of one of these fault scarps. The calculated ages for profiles 3 (Soldier Pass), 4, 4B, and 5A do not overlap, at the 1σ level, with all the other calculated profile ages and are therefore not included in the calculation of the weighted mean elapsed time since the last rupture. Profile 4B crosses a fault scarp cut by small channels and profile 3 crosses a composite scarp; both profiles therefore may violate the modeling condition that material transport is dominated by slope processes, and thus the calculated age deviates from the others. There are no apparent geomorphic features that explain the difference in calculated age of profiles 4 and 5A.

The most recent set of fault scarps along the Deep Springs fault extends for ~20 km from the southern margin of Deep Springs Lake to southwest of Chocolate Mountain (Fig. 2A). The fault scarps are well defined within the unconsolidated, coarse granitic-derived sand of Qf1 as well as at the interface of alluvial fan deposits and bedrock. The large landslide to the southeast of Deep Springs College, a series of debris flows, Qdf, and recent stream sand and gravel, Qal, have been deposited across these fault scarps (Fig. 2, A, B, and C). Topographic profiling of 16 fault scarps developed within Qf1, 6 from the westernmost fault scarps west of Soldier Pass and 10 from the graben east of Deep Springs College (Fig. 2, D and E), shows that these are not composite scarps (Fig. 7). Therefore, the average surface offset (Fig. 6) of 2.7 ± 0.9 m measured on these scarps is the result of a single rupture event.

The radiocarbon age of 1.960 ± 0.055 ka (sample 95-54C; Fig. 2A) from a fragment of detrital charcoal within Qf1 deposits provides a maximum age for the most recent ground-rupturing earthquake. We have also estimated the age of young fault scarps by using morphologic dating. Morphologic dating compares model profiles to observed profiles (e.g., Arrowsmith et al., 1998; Arrowsmith, 1995; Nash, 1986; Hanks et al., 1984). The development of the observed profile is a function of time, *t*, and the value of the rate constant or diffusivity, κ (m^2/k.y.); the morphologic age is the product of these two variables, κ*t* (m^2) (Arrowsmith et al., 1998; Arrowsmith, 1995; Hanks et al., 1984). Therefore, if we have an independent estimate of κ, we can determine *t*, or alternatively, if we have an independent estimate of *t*, we can determine κ. To determine the morphologic age of the fault scarp, we forward-model initial profiles, using the numerical method of Arrowsmith (1995) and Arrowsmith et al. (1996), and iterate the morphologic age until a best fit is obtained between model and observed profile (Fig. 8A). A root mean square (RMS) of the misfit between the model profile and the observed profile is determined (Avouac, 1993; Arrowsmith et al., 1998). A plot of RMS versus morphologic age (Fig. 8B) passes through a well-defined minimum (RMS_{min}); the uncertainty of the model fit is determined by defining confidence intervals on the best-fitting profile for those that fit the observations within 5 cm of RMS_{min} (Avouac, 1993; Arrowsmith et al., 1998). If we specify a diffusivity constant we can calculate the elapsed time for the initial scarp to degrade to the observed scarp. For scarps in Deep Springs Valley, we have chosen a value of 1.1 m^2/k.y., which was shown by Hanks et al. (1984) to be generally applicable, as a first approximation, to the modification of unconsolidated alluvial shoreline scarps of Lake Bonneville. To model a set of fault scarps successfully, the following conditions and assumptions must be met (Arrowsmith, 1995; Arrowsmith et al., 1998).

1. There are no subsequent changes in elevation following the rupture event.

2. There is more material available for erosion than transport processes are able to take away and the material must be unconsolidated.

3. No material is transported in or out of the profile.

4. Material transport rate is proportional to the local slope, and this process is dominated by rain splash, animal-induced disturbances, and soil creep.

5. Normal fault scarps developed in unconsolidated alluvial deposits typically slump to the angle of repose (35°) within a few hundred years after a surface rupture event (e.g., Arrowsmith and Rhodes, 1994; Hanks and Andrews, 1989; Wallace, 1980). Because this is not a diffusive process, we assume, for modeling purposes, that it occurs relatively rapidly after the formation of the scarp.

Diffusion erosion modeling of the profiles measured across the scarps west of Soldier Pass and east of Deep Springs College (Figs. 2, D and E, 7, and 8) yield morphologic ages that range from 0.4 m^2 to 9.0 m^2, with a weighted mean morphologic age of 1.9 ± 0.5 m^2 (Table 3). Assuming a diffusivity value of κ = 1.1 m^2/k.y. yields a weighted mean elapsed time since the scarp-forming event of 1.7 ± 0.5 k.y. (Table 3; Fig. 9). The age determined from diffusion erosion modeling is consistent, within 1σ error, with the charcoal age. Therefore, we conclude that the most re-

cent earthquake along the Deep Springs fault occurred ~1800 yr ago.

From the surface expression of this most recent fault scarp, we can assess the seismic moment (M_o) and moment magnitude (M_w) for this earthquake. The seismic moment is defined as $M_o = \mu SA$ (Hanks et al., 1975), where μ = shear modulus, S = magnitude of slip, and A = area of slip. If we assume an initial fault dip of 60°, consistent with the Coulomb law of failure for normal faults, an average surface offset of 2.7 m yields a dip-slip magnitude of 3.1 m. Given a fault rupture length of ~20 km, a depth of 15 km, the characteristic depth for large normal fault earthquakes within the Basin and Range Province (Rogers et al., 1991), and 60° fault dip, yields a fault rupture area of 345 km^2. Using an average shear modulus, $\mu = 3 \times 10^{11}$ dyne-cm, yields an estimated seismic moment, $M_o = 3.2 \times 10^{26}$. To calculate moment magnitude, M_w, we use the equation of Hanks and Kanamori (1979), $M_w = 2/3 \log M_o - 10.7$, which yields an estimated $M_w = 7.0$ for the most recent earthquake.

On the basis of a large empirical database, Wells and Coppersmith (1994) developed a set of equations that relate M_w to rupture length, average displacement, and maximum displacement. Using these equations for a rupture length of 20 km, average surface offset of 2.7 m, and maximum surface offset of 4.6 m (Table 3) yields an estimated M_w that ranges from 6.6 to 7.3 for the Deep Springs fault.

Assuming that a surface offset of 2.7 ± 0.9 m is characteristic of surface rupture along the Deep Springs fault and that the ~0.9 mm/yr vertical slip rate since the eruption of the Bishop Tuff estimated for the fault east of Deep Springs College holds for the entire Deep Springs fault, then the recurrence interval for earthquakes with a $M_w \approx 7.0$ is 2–4 k.y.

TABLE 3. SUMMARY OF FAULT SCARP AGE FOR THE YOUNGEST FAULT SCARPS ALONG THE DEEP SPRINGS FAULT

Profile number	κt(m²)	+Δκt	–Δκt	Age (ka)*	±Δ age (ka)*	RMS (m)	Scarp angle	Surface offset
West of Soldier Pass								
1a	7.2	6.8	4.0	6.5	6.2	0.05	14	2.2
2	8.2	11.8	5.8	7.5	5.3	0.03	15	1.7
3*	0.4	1.8	0.2	0.4	0.2	0.02	18	2.7
4*	9.0	9.4	5.4	8.2	4.9	0.05	21	2.8
5	8.0	7.6	4.6	7.3	6.9	0.04	19	2.4
6	3.2	5.8	2.0	2.9	1.8	0.05	12	3.3
East of Deep Springs College								
1	4.4	4.2	2.4	4.0	3.8	0.03	21	2.4
2a	2.4	4.8	2.0	2.2	1.8	0.05	22	1.8
2b	2.8	3.6	2.0	2.5	1.8	0.05	21	1.7
3	2.8	2.4	1.6	2.5	2.2	0.03	28	3.0
4a	4.6	3.8	2.6	4.2	3.5	0.05	27	3.3
4b†	15.8	15.8	8.8	14.4	8.0	0.11	20	2.4
5a†	18.9	8.4	6.3	17.2	7.6	0.05	20	3.9
6a	1.2	2.0	1.0	1.1	0.9	0.04	30	3.2
6b	1.2	2.0	0.8	1.1	0.7	0.02	8	1.3
7a	2.6	2.2	1.8	2.4	2.0	0.60	32	4.6

*Age and its uncertainty, ±Δ age, is the elasped time since the fault scarp forming event and is determined by dividing the κτ value (i.e. morphologic age) by the calculated κ value of 1.1 m²/k.y. determined from Lake Bonneville shoreline scarps (Hanks et al., 1984).

†The calculated ages for these profiles do not overlap, at the 1σ level, with all of the other calculated profile ages and are therefore not included in the calculation of the weighted mean morphologic age and weighted mean elapsed time of 1.9 ± 0.5 m² and 1.7 ± 0.5 k.y., respectively. See Figure 9 caption for more details.

REGIONAL KINEMATICS

A recently proposed model for the eastern California shear zone in the Death Valley–Owens Valley regions (Fig. 1A) suggests that the kinematic framework of this zone is changing rapidly (Dixon et al., 1995). This kinematic model predicts that the locus of right-lateral shear has shifted or is in the process of shifting from the Death Valley fault zone to the Owens Valley fault zone. Furthermore, the model suggests that northeast-striking, northwest-dipping normal faults, such as the Deep Springs fault, Eureka Valley faults, and Towne Pass–Emigrant fault system, transfer slip from the Owens Valley and Hunter Mountain–Panamint Valley fault zones to the northern Death Valley–Furnace Creek and Fish Lake Valley fault zones (Fig. 1A). This model also predicts that slip along these normal faults progresses from southeast to northwest; the Towne Pass–Emigrant fault system is the oldest and currently least active, whereas the Deep Springs fault is the youngest and currently most active.

The Deep Springs fault, as well as the other northeast-striking, northwest-dipping normal faults, defines right steps between the Owens Valley, Hunter Mountain–Panamint Valley, and Death Valley–Furnace Creek–Fish Lake Valley fault zones (Fig. 1A). Right steps in the Death Valley and Hunter Mountain–Panamint Valley fault zones are associated with the Death Valley and Panamint Valley pull-apart basins, respectively (Burchfiel et al., 1987; Burchfiel and Stewart, 1966; Oswald, 1998), and Deep Springs Valley is analogous to these larger basins. Our work shows that the Deep Springs fault is a young and currently active normal fault, thus supporting one aspect of the model. However, seismicity and geomorphic evidence for young slip indicate that the other normal faults are also still active, and therefore these faults define a zone of distributed deformation between subparallel strike-slip faults (Fig. 1A). Fault slip is still occurring on the Panamint Valley–Hunter Mountain system (Fig. 1). Zhang et al. (1990) reported a Holocene slip rate of 2.4 ± 0.8 mm/yr for the southern Panamint fault, and Oswald (1998) established that fault scarps along the Hunter Mountain fault system crosscut Holocene deposits, as do right-stepping normal faults at the northern end of the fault system in Saline Valley. The May 17, 1993, $M_W = 6.1$ Eureka Valley earthquake on a normal fault (CalTech TERRAscope solution; Massonnet and Feigl, 1995; Peltzer and Rosen, 1995) confirms that this segment of the distributed zone of deformation is still active. Furthermore, a fault scarp, with an average surface offset of 1.8 ± 0.7 m, cuts Holocene deposits along the eastern part of the Towne Pass fault (J. Lee, unpublished mapping), indicating that this fault is also still active. These observations are consistent with geodetic data that suggest that the Owens Valley, Fish Lake Valley, Hunter Mountain, and Death Valley fault zones are currently active and have estimated slip rates of 3.0 ± 1.9 mm/yr, 8.4 ± 2.0 mm/yr, 1–3 mm/yr, and 3–5 mm/yr, respectively (Bennett et al., 1997; Savage and Lisowski, 1995; Dixon et al., 2000).

Initiation of slip along these normal faults, however, appears to young to the northwest. Geologic mapping along the Towne Pass–Emigrant fault system suggests that the Towne Pass fault is a splay in the hanging wall of the Emigrant detachment fault (Hodges et al., 1989). Hall (1971) and Hodges et al. (1989) inferred that deposition in the hanging wall of the Towne Pass fault began after 3.6 Ma, thus providing an upper age limit for motion along this fault. Slip along the Emigrant fault initiated at least as early as 11.4 Ma and continued to ca. 3.4 Ma (Snyder and Hodges,

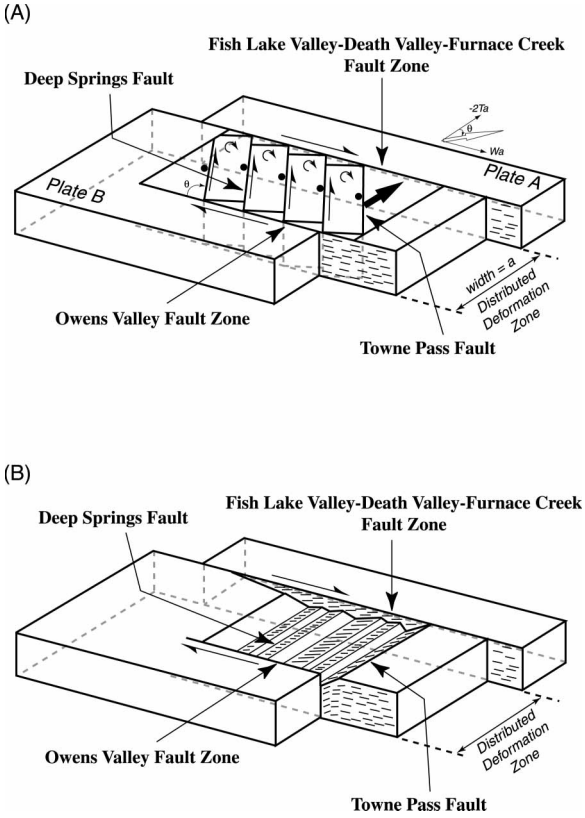

Figure 10. Schematic block diagrams illustrating two potential mechanisms of slip transfer between subparallel strike-slip faults and connecting normal faults. (A) Floating or pinned block model of McKenzie and Jackson (1983, 1986). Two rigid plates, A and B, bound a zone of distributed deformation with width *a*. The relative motion between the two plates is given by the large white arrow defined by two components: $-2Ta$ orthogonal to the zone and *Wa* parallel to the zone. Motion across fault blocks within the zone of distributed deformation is perpendicular to the zone boundaries and is shown by the large black arrow. Fault blocks rotate clockwise (as shown) with an angular velocity of *W* and *W*/2 for the pinned and floating block models, respectively. θ is the angular orientation between fault blocks and zone boundaries. See text for discussion. (B) A displacement-transfer or fault-step geometry between two subparallel strike-slip faults and connecting normal faults modified from Oldow et al. (1994). In this model the magnitude of extension along the normal faults is proportional to the amount of strike-slip motion transferred.

2000), considerably earlier than along the Deep Springs fault. Initiation of slip along the normal faults in the region between these two fault systems, however, is unknown.

Two models can potentially explain the mechanism of slip transfer between subparallel strike-slip faults and connecting normal faults (Fig. 10). The first is the two-dimensional block-rotation model, either with pinned or with floating blocks, of McKenzie and Jackson (1983, 1986) (Fig. 10A). In the pinned model, fault blocks are pinned to the boundaries of the deforming zone (McKenzie and Jackson, 1986), whereas in the floating model, fault-block lengths are small compared to the width of the deforming zone and fault blocks float within the zone (McKenzie and Jackson, 1983). In both models, fault movement and block rotation within a zone of distributed deformation accommodate strike-slip motion between rigid plates. Using the block-rotation model as an analogue, the rigid plates are defined as the blocks to the east of the Fish Lake Valley fault zone and to the west of the Owens Valley fault zone (Fig. 10A). The relative motion between the two plates must be transtensional in order for extension to occur across the fault blocks, and is given by the large white arrow in Figure 10A, defined by two components: $-2Ta$ orthogonal to the zone and *Wa* parallel to the zone. The angular velocity of the blocks is *W* for the pinned-block model and *W*/2 for the floating-block model (Fig. 10A). Dixon et al. (2000) estimated a present-day extension rate of 1.2 ± 1.4 mm/yr perpendicular to the zone and a total right-lateral slip rate across the zone of 11.4 ± 1.1 mm/yr; thus transtensional motion is permissible. In both the pinned and floating models, motion across fault blocks in the deforming zone is perpendicular to zone boundaries (defined by the large black arrow in Fig. 10A). Therefore, a key component of this model is that movement along normal faults should be oblique (left lateral and dip slip), and faults and fault blocks should undergo clockwise rotation. However, our work has established that slip along the Deep Springs fault is essentially downdip, and slip along the Towne Pass fault is also downdip (Hodges et al., 1989; Lee, unpublished mapping), clearly showing that neither block-rotation model adequately explains the transfer of slip between subparallel strike-slip faults.

The second model is a modification of the low-angle displacement-transfer system of Oldow et al. (1994) (Fig. 10B). In this model, high-angle normal faults describe a right-stepping geometry in which the magnitude of extension is proportional to the amount of strike-slip motion transferred. Therefore, the Deep Springs fault transfers ~0.7 mm/yr of slip from the Owens Valley fault zone to the Fish Lake Valley fault zone. This represents transfer of ~15%–65% of present-day slip along the Owens Valley fault. Continuation of as little as 45% of Owens Valley fault motion northward along the White Mountains fault zone is allowable because this section of the White Mountains fault zone contains some geomorphic evidence for strike-slip faulting, such as deflected stream channels and shutter ridges (dePolo, 1989). The White Mountains fault zone also underwent a series of primarily strike-slip earthquakes between July and September 1986, including five earthquakes with magnitude (M_L) >5 (the Chalfant Valley earthquake sequence) (Cockerham and Corbett, 1987). However, dePolo (1989) described only one locality that shows alluvial landforms offset right laterally, suggesting that right-lateral offsets of alluvial units are scarce. Because geomorphic evidence for strike-slip deformation along the White Mountains fault zone is relatively scarce, especially compared to the Owens Valley fault zone (cf. dePolo, 1989; Beanland and Clark, 1994), we suggest that much of Owens Valley fault slip is transferred eastward to the Fish Lake Valley fault zone via the Deep Springs fault by a displacement-transfer mechanism.

Within this zone of distributed deformation, the other normal fault systems, such as the Towne Pass fault and Eureka Valley faults

(Fig. 1A), have similar orientations, apparent downdip slips, and settings, suggesting that all these normal faults transfer slip between subparallel strike-slip faults via a displacement-transfer mechanism, as shown in Figure 10B.

CONCLUSIONS

The Deep Springs fault is a northeast-striking, northwest-dipping normal fault that developed along the southeastern edge of the Deep Springs Valley, an enclosed basin within the White and Inyo mountains. The Deep Springs fault cuts a basement of pre-Cenozoic rocks as well as Quaternary alluvial deposits, tuffs, and basalts. We estimate that slip along the fault began ca. 1.7 Ma at a horizontal extension rate of ~0.7 mm/yr. The fault is characterized by multiple fault planes and fault scarps that become progressively younger toward the sedimentary basin. The youngest set of fault scarps cuts across Holocene alluvial fan deposits and yields an average surface offset of 2.7 m. Diffusion erosion modeling of these fault scarps and radiocarbon analyses on detrital charcoal found in the footwall of one of these scarps indicates that the most recent surface rupture occurred ~1800 yr ago. This earthquake ruptured an ~20 km section of the fault, implying that the M_w was ~7.0. The Deep Springs fault is a displacement-transfer normal fault exposed between two subparallel right-lateral strike-slip faults, the Owens Valley fault and the Fish Lake Valley fault zone. This normal fault is one of several displacement-transfer normal faults within a broad zone of diffuse deformation that accommodates ~24% of Pacific–North American relative plate motion.

ACKNOWLEDGMENTS

We thank Tim Dixon for getting us involved in the problem of the kinematics of recent faulting within this part of the eastern California shear zone. We are grateful to the many people who assisted us in the field, including Tim Dixon, Chris Walls, and Doug Yule, Central Washington University undergraduate students Ken Austin, Will Blanton, Ana Cadena, Erik Johansen, and Sam VanLaningham, and especially Andrew Miner for his keen field observations. Sally McGill kindly loaned her Wild total station for some of our surveys. We thank Lynda Holland for the mineral separates. Special thanks to Matt Heizler for completing one of our Ar/Ar analyses on very short notice. Phil Gans provided use of his Ar/Ar laboratory at University of California, Santa Barbara. G. Burr performed the radiocarbon analyses at the National Science Foundation supported Accelerator Mass Spectrometer Laboratory, Department of Physics, University of Arizona. The community at Deep Springs College, especially the Szewczak family, provided warm hospitality, a place to pitch our tents, and fine dinners during our field studies. Many discussions with Ramon Arrowsmith, Tim Dixon, Chris Walls, and Doug Yule contributed to this work. Excellent reviews by William Bryant, Doug Burbank, Tom Hanks, and Marith Reheis improved this manuscript. We thank Ramon Arrowsmith and Frank Spera for providing the software and hardware, respectively, for the diffusion erosion modeling. Stereonet software used in this manuscript was created by Rick Allmendinger. This research was supported by National Science Foundation grants EAR-95–06688 and EAR-95-26016.

REFERENCES CITED

Arrowsmith, J.R., 1995, Coupled tectonic deformation and geomorphic degradation along the San Andreas fault system [Ph.D. dissert.]: Stanford, California, Stanford University, 346 p.

Arrowsmith, J.R., and Rhodes, D.D., 1994, Original forms and initial modifications of the Galway Lake Road scarp formed along the Emerson fault during the June 28, 1992, Landers, California, earthquake: Seismological Society of America Bulletin, v. 84, p. 511–527.

Arrowsmith, J.R., Pollard, D.D., and Rhodes, D.D., 1996, Hillslope development in areas of active tectonics: Journal of Geophysical Research, v. 101, p. 6255–6275.

Arrowsmith, J.R., Rhodes, D.D., and Pollard, D.D., 1998, Morphologic dating of scarps formed by repeated slip events along the San Andreas fault, Carrizo Plain, California: Journal of Geophysical Research, v. 103, p. 10141–10160.

Avouac, J.-P., 1993, Analysis of scarp profiles: Evaluation of errors in morphologic dating: Journal of Geophysical Research, v. 98, p. 6745–6754.

Beanland, S., and Clark, M.M., 1994, The Owens Valley fault zone, eastern California, and surface rupture associated with the 1872 earthquake: U.S. Geological Survey Bulletin 1982, 29 p.

Bennett, R.A., Wernicke, B.P., Davis, J.L., Elosegui, P., Snow, J.K., Abolins, M.J., House, M.A., Stirewalt, G.L., and Ferrill, D.A., 1997, Global positioning system constraints on fault slip rates in the Death Valley region, California and Nevada: Geophysical Research Letters, v. 24, p. 3073–3076.

Brogan, G.E., Kellogg, K.S., Slemmons, D.B., and Terhune, C.L., 1991, Late Quaternary faulting along the Death Valley–Furnace Creek fault system, California and Nevada: U.S. Geological Survey Bulletin 1991, 23 p.

Bryant, W.A., 1989, Deep Springs fault, Inyo County, California, an example of the use of relative-dating techniques: California Geology, v. 42, p. 243–255.

Burchfiel, B.C., and Stewart, J.H., 1966, "Pull-apart" origin of the central segment of Death Valley, California: Geological Society of America Bulletin, v. 77, p. 439–442.

Burchfiel, B.C., Hodges, K.V., and Royden, L.H., 1987, Geology of Panamint Valley–Saline Valley pull-apart system, California: Palinspastic evidence for low-angle geometry of a Neogene range-bounding fault: Journal of Geophysical Research, v. 92, p. 10422–10426.

Butler, P.R., Troxel, B.W., and Verosub, K.L., 1988, Late Cenozoic history and styles of deformation along the southern Death Valley fault zone, California: Geological Society of America Bulletin, v. 100, p. 402–410.

Cockerham, R.S., and Corbett, E.J., 1987, The 1986 Chalfant Valley, California, earthquake sequence: Preliminary results: Seismological Society of America Bulletin, v. 77, p. 280–289.

Dalrymple, G.B., 1963, Potassium-argon dates of some Cenozoic volcanic rocks of the Sierra Nevada, California: Geological Society of America Bulletin, v. 74, p. 379–390.

dePolo, C.M., 1989, Seismotectonics of the White Mountain fault system, eastern California and western Nevada [Master's thesis]: Reno, University of Nevada, 354 p.

Dixon, T.H., Robaudo, S., Lee, J., and Reheis, M.C., 1995, Constraints on present-day Basin and Range deformation from space geodesy: Tectonics, v. 14, p. 755–772.

Dixon, T.H., Miller, M., Farina, F., Wang, H., and Johnson, D., 2000, Present-day motion of the Sierra Nevada block, and some tectonic implications for the Basin and Range province, North American Cordillera: Tectonics, v. 19, p. 1–24.

Dokka, R.K., and Travis, C.J., 1990a, Late Cenozoic strike-slip faulting in the Mojave Desert, California: Tectonics, v. 9, p. 311–340.

Dokka, R.K., and Travis, C.J., 1990b, Role of the eastern California shear zone in accommodating Pacific–North American plate motion: Geophysical Research Letters, v. 17, p. 1323–1326.

Hacker, B.R., 1993, Evolution of the northern Sierra Nevada metamorphic belt: Petrologic, structural, and Ar/Ar constraints: Geological Society of America Bulletin, v. 105, p. 637–656.

Hall, W.E., 1971, Geology of the Panamint Butte Quadrangle, Inyo County, California: U.S. Geological Survey Bulletin 1299, 67 p.

Hanks, T.C., and Andrews, D.J., 1989, Effect of far-field slope on morphologic dating of scarplike landforms: Journal of Geophysical Research, v. 94, p. 565–573.

Hanks, T.C., and Kanamori, H., 1979, A moment magnitude scale: Journal of Geophysical Research, v. 84, p. 2348–2350.

Hanks, T.C., Hileman, J.A., and Thatcher, W., 1975, Seismic moments of the larger earthquakes of the southern California region: Geological Society of America Bulletin, v. 86, p. 1131–1139.

Hanks, T.C., Bucknam, R.C., Lajoie, K.R., and Wallace, R.E., 1984, Modification of wave-cut and fault controlled landforms: Journal of Geophysical Research, v. 89, p. 5771–5790.

Hodges, K.V., McKenna, L.W., Stock, J., Knapp, J., Page, L., Sternlof, K., Silverberg, D., Wust, G., and Walker, J.D., 1989, Evolution of extensional basins and Basin and Range topography west of Death Valley, California: Tectonics, v. 8, p. 453–467.

Humphreys, E.D., and Weldon, R.J.I., 1994, Deformation across the western United States: A local estimate of Pacific–North America transform deformation: Journal of Geophysical Research, v. 99, p. 19975–20010.

Izett, G.A., and Obradovitch, J.D., 1994, $^{40}Ar/^{39}Ar$ constraints for the Jaramillo normal subchron and the Matuyama-Brunhes geomagnetic boundary: Journal of Geophysical Research, v. 99, p. 2925–2934.

Lustig, L.K., 1965, Clastic sedimentation in Deep Springs Valley, California: U.S. Geological Survey Professional Paper, v. 352-F, p. 131–192.

Machette, M.N., Personius, S.F., Nelson, A.R., Schwartz, D.P., and Lund, W.R., 1991, The Wasatch fault zone, Utah—Segmentation and history of Holocene earthquakes: Journal of Structural Geology, v. 13, p. 137–150.

Massonnet, D., and Feigl, K.L., 1995, Satellite radar interferometric map of the coseismic deformation field of the M = 6.1 Eureka Valley, California, earthquake of May 17, 1993: Geophysical Research Letters, v. 22, p. 1541–1544.

McKee, E.H., and Nelson, C.A., 1967, Geologic map of the Soldier Pass quadrangle, California and Nevada: U.S. Geological Survey Geologic Quadrangle Map GQ-654, scale 1:62 500.

McKenzie, D., and Jackson, J., 1983, The relationship between strain rates, crustal thickening, paleomagmatism, finite strain and fault movements within a deforming zone: Earth and Planetary Science Letters, v. 65, p. 182–202.

McKenzie, D., and Jackson, J., 1986, A block model of distributed deformation by faulting: Jounral of the Geological Society of London, v. 143, p. 349–353.

Miller, W.J., 1928, Geology of Deep Springs Valley, California: Journal of Geology, v. 36, p. 510–525.

Nash, D.B., 1986, Morphologic dating and modeling degradation of fault scarps, *in* Wallace, R.E., ed., Active Tectonics: Washington, D.C., National Academy Press, p. 181–194.

Nelson, C.A., 1966a, Geologic map of the Waucoba Mountain Quadrangle, Inyo County, California: U.S. Geo-

logical Survey Geologic Quadrangle Map GQ-528, scale 1:62 500.

Nelson, C.A., 1966b, Geologic map of the Blanco Mountain quadrangle, Inyo and Mono Counties, California: U.S. Geological Survey Geologic Quadrangle Map GQ-529, scale 1:62 500.

Oldow, J.S., Kohler, G., and Donelick, R.A., 1994, Late Cenozoic extensional transfer in the Walker Lane strike-slip belt, Nevada: Geology, v. 22, p. 637–640.

Oswald, J.A., 1998, Quaternary geology of southern Saline Valley and neotectonic character of the Hunter Mountain fault zone [Master's thesis]: Reno, University of Nevada, 69 p.

Peltzer, G., and Rosen, P., 1995, Surface displacement of the 17 May 1993 Eureka Valley, California, earthquake observed by SAR interferometry: Science, v. 268, p. 1333–1336.

Reheis, M.C., 1992, Geologic map of late Cenozoic deposits and faults in parts of the Soldier Pass and Magruder Mountain 15′ quadrangles, Inyo and Mono counties, California, and Esmeralda County, Nevada: U.S. Geological Survey Miscellaneous Investigations Map I-2268, scale 1:24 000.

Reheis, M.C., and Sawyer, T.L., 1997, Late Cenozoic history and slip rates of the Fish Lake Valley, Emigrant Peak, and Deep Springs fault zones, Nevada and California: Geological Society of America Bulletin, v. 109, p. 280–299.

Rogers, A.M., Harmsen, S.C., Corbett, E.J., Priestley, K., and dePolo, D., 1991, The seismicity of Nevada and some adjacent parts of the Great Basin, *in* Slemmons, D.B., et al., eds., Neotectonics of North America: Boulder, Colorado, Geological Society of America, Decade Map Volume 1, p. 153–184.

Sauber, J., Thatcher, W., Solomon, S.C., and Lisowski, M., 1994, Geodetic slip rate for the eastern California shear zone and the recurrence time of Mojave desert earthquakes: Nature, v. 367, p. 264–266.

Savage, J.C., and Lisowski, M., 1984, Deformation in the White Mountain seismic gap, California-Nevada, 1972–1982: Journal of Geophysical Research, v. 89, p. 7671–7687.

Savage, J.C., and Lisowski, M., 1995, Strain accumulation in Owens Valley, California: Seismological Society of America Bulletin, v. 85, p. 151–158.

Savage, J.C., Lisowski, M., and Prescott, W.H., 1990, An apparent shear zone trending north-northwest across the Mojave Desert into Owens Valley, eastern California: Geophysical Research Letters, v. 17, p. 2113–2116.

Snyder, N.P., and Hodges, K.V., 2000, Depositional and tectonic evolution of a superdetachment basin: $^{40}Ar/^{39}Ar$ geochronology of the Nova Formation, Panamint Range, California: Basin Research, v. 12, p. 19–30.

Stuiver, M., and Pollach, H.A., 1977, Discussion; reporting of C-14 data: Radiocarbon, v. 19, p. 355–363.

Stuiver, M., and Reimer, P.J., 1993, Extended ^{14}C data base and revised CALIB 3.0 ^{14}C age calibration program: Radiocarbon, v. 35, p. 215–230.

Wallace, R.E., 1980, Degradation of the Hebgen Lake fault scarps of 1959: Geology, v. 8, p. 225–229.

Wang, H., Dixon, T., and Donnellan, A., 1994, Where is the eastern California shear zone north of 37° latitude? [abs.]: Eos (Transactions, American Geophysical Union), v. 75, p. 182.

Wells, D.L., and Coppersmith, K.J., 1994, New empirical relationships among magnitude, rupture length, rupture width, rupture area, and surface displacement: Seismological Society of America Bulletin, v. 84, p. 974–1002.

Wills, C.J., 1989, A neotectonic tour of the Death Valley fault zone, Inyo County: California Geology, v. 42, p. 195–200.

Wills, C.J., 1996, Liquefaction in the California desert; an unexpected hazard: California Geology, v. 49, p. 31–35.

Wilson, D.V., 1975, Geophysical investigation of the subsurface structure of Deep Springs Valley, California [Master's thesis]: Los Angeles, University of California, 65 p.

Zhang, P., Ellis, M., Slemmons, D.B., and Mao, F., 1990, Right-lateral displacements and the Holocene slip rate associated with prehistoric earthquakes along the southern Panamint Valley fault zone: Implications for southern Basin and Range tectonics and coastal California deformation: Journal of Geophysical Research, v. 95, p. 4857–4872.

MANUSCRIPT RECEIVED BY THE SOCIETY AUGUST 19, 1999
REVISED MANUSCRIPT RECEIVED MAY 5, 2000
MANUSCRIPT ACCEPTED AUGUST 24, 2000

Printed in the USA